Astronomy & Astrophysics manuscript no.
(will be inserted by hand later)

Spectroscopic determination of photospheric parameters and chemical abundances of 6 K-type stars*,**

L. Affer[1], G. Micela[1], T. Morel[1], J. Sanz-Forcada[1,2], and F. Favata[2]

[1] Istituto Nazionale di Astrofisica, Osservatorio Astronomico di Palermo G. S. Vaiana, Piazza del Parlamento 1, 90134 Palermo, Italy
e-mail: affer@astropa.unipa.it

[2] Astrophysics Division - Research and Science Support Department of ESA, ESTEC, Postbus 299, 2200 AG Noordwijk, The Netherlands

Received 17 May 2004 / Accepted 16 November 2004

Abstract. High resolution, high-S/N-ratio optical spectra have been obtained for a sample of 6 K-type dwarf and subgiant stars, and have been analysed with three different LTE methods in order to derive detailed photospheric parameters and abundances and to compare the characteristics of analysis techniques. The results have been compared with the aim of determining the most robust method to perform complete spectroscopic analyses of K-type stars, and in this perspective the present work must be considered as a pilot study. In this context we have determined the abundance ratios with respect to iron of several elements. In the first method the photospheric parameters ($T_{\rm eff}$, $\log g$, and ξ) and metal abundances are derived using measured equivalent widths and Kurucz LTE model atmospheres as input for the MOOG software code. The analysis proceeds in an iterative way, and relies on the excitation equilibrium of the Fe I lines for determining the effective temperature and microturbulence, and on the ionization equilibrium of the Fe I and Fe II lines for determining the surface gravity and the metallicity. The second method follows a similar approach, but discards the Fe I low excitation potential transitions (which are potentially affected by non-LTE effects) from the initial line list, and relies on the $B-V$ colour index to determine the temperature. The third method relies on the detailed fitting of the 6162 Å Ca I line to derive the surface gravity, using the same restricted line list as the second method. Methods 1 and 3 give consistent results for the program stars; in particular the comparison between the results obtained shows that the Fe I low-excitation potential transitions do not appear significantly affected by non-LTE effects (at least for the subgiant stars), as suggested by the good agreement of the atmospheric parameters and chemical abundances derived. The second method leads to systematically lower $T_{\rm eff}$ and $\log g$ values with respect to the first one, and a similar trend is shown by the chemical abundances (with the exception of the oxygen abundance). These differences, apart from residual non-LTE effects, may be a consequence of the colour-$T_{\rm eff}$ scale used. The α-elements have abundance ratios consistent with the solar values for all the program stars, as expected for "normal" disk stars. The first method appears to be the most reliable one, as it is self-consistent, it always leads to convergent solutions and the results obtained are in good agreement with previous determinations in the literature.

Key words. stars:individual: HD 4628 - stars:individual: HD 10780 - stars:individual: HD 23249 (δ Eri) - stars:individual: HD 198149 (η Cep) - stars:individual: HD 201091 (61 Cyg A) - stars:individual: HD 222404 (γ Cep)

1. Introduction

The accurate determination of the chemical composition of the atmospheres of stars belonging to different populations and different evolutionary stages allows us to study the enrichment history of the interstellar matter and, combined with kinematical data and ages, provides a powerful way of probing the chemical and dynamical evolution of the Galaxy. Unevolved low-mass stars yield information about the chemical composition of the Galactic material from which they were formed, since their abundances are not affected by the nuclear reactions occurring in their cores and therefore are the ideal tracers of the Galactic chemical evolution and a key indicator (with kinematics) of which population they belong to. Nevertheless the procedures used to determine the abundances are still not standard, and often rather complicated. In fact, even for the Sun, which is the only star for which redundant information concerning its chemical composition can be obtained from various sources like the photosphere, chromosphere, corona, meteorites, and so on, the iron abundance is still a matter of debate (Grevesse & Sauval 1999). Only during the last two decades

* Based on observations made with the Nordic Optical Telescope, operated on the island of La Palma jointly by Denmark, Finland, Iceland, Norway, and Sweden, in the Spanish Observatorio del Roche de los Muchachos of the Instituto de Astrofisica de Canarias.

** Table 6 is only available in electronic form at http://www.edpsciences.org has it been demonstrated that the solar photospheric composition agrees remarkably well with that of meteorites (Grevesse & Noels 1993; Grevesse & Sauval 1999). The main cause of the difficulties encountered is the lack of accurate transition probabilities for all the iron lines.

A complete description of the chemical abundances of disk stars implies obtaining and analysing high-resolution spectra for a significant number of stars carefully selected to be a statistically representative sample of this population. This implies, as a consequence, the necessity of developing an efficient method for spectroscopic determinations of atmospheric parameters, by which the effective temperature ($T_{\rm eff}$), the surface gravity ($\log g$), the microturbulent velocity (ξ), and the metallicity (which is often represented by the abundance of iron relative to the Sun, i.e. [Fe/H]), can be determined in a robust way. There are several different analysis techniques used until now, most of them relying on photometry (although it has been recognized that some of the employed photometric indices may be seriously affected by chromospheric activity, e.g. Favata et al. 1997); some are based on the comparison between synthetic and observed spectra (when high quality, high resolution data are available; Edvardsson 1988) or upon other different spectroscopic approaches (spectral line-depth ratios as temperature indicators for cool stars, for instance; Gray 1994), and so on. It is not clear to what extent these many different techniques are consistent one with the other. Consistency checks often involve the determination of stellar parameters by two or more methods.

Aiming at deriving the photospheric parameters and metal abundances from the stellar spectra themselves in a self-consistent way, we have applied, to a small sample of high signal-to-noise (S/N) ratio spectra of nearby stars, three analysis techniques, which have been compared in order to establish their respective merits and drawbacks. The first method uses the excitation equilibrium of neutral iron lines to determine the effective temperature, and the ionization equilibrium of the Fe I and Fe II lines to determine the surface gravity and metallicity. The second method proceeds like the first one but relies on the $B-V$ colour index to determine the effective temperature, and discards the low excitation potential transitions in order to avoid possible non-LTE effects. The third method proceeds like the first two methods, by iteration, but determines the surface gravity from the detailed fitting of the 6162 Å Ca I line, and uses the ionization equilibrium of Fe I and Fe II lines to determine, this time, the effective temperature. The third method can be used only for stars for which very-high-quality spectroscopic data are available. Very high spectral resolution is necessary for studying late-type stars, whose spectra are very crowded with lines. The high resolution, high S/N ratio observations in the present work can provide accurate equivalent widths (EWs) for detailed abundance analysis based on the reliable continuum locations and well separated lines in the spectra.

Most of the previous works devoted to the study of stellar abundances of large numbers of dwarf and subgiant stars with known kinematics and derived ages (Feltzing & Gustafsson 1998; Fuhrmann 1998; Chen et al. 2000), have been concerned with the warmer F and G dwarf stars. In this paper we investigate, by means of detailed spectroscopic analyses, the iron abundance as well as the abundance of several elements for 6 dwarf and subgiant nearby K-type stars. The present work has to be considered as a pilot program for the study of K-type stars, for which detailed spectroscopic abundance analyses are still rare. This work is related to the studies of Katz et al. (2003) and Morel et al. (2003, 2004) who analysed samples of active K stars. In the present paper we will analyse "normal" quiet K stars. The paper is organized as follows: in Sects. 2 and 3 we describe the observations and methods of analysis in detail and present the derived abundances: the results, as well as ages and kinematics, are discussed in Sect. 4 and compared to those of other works and, finally, Sect. 5 summarizes our findings.

Table 1. Spectral type, visual apparent magnitudes, colour indices, number of exposures (N), and mean resulting signal-to-noise ratios (at $\lambda \approx$ 6000 Å) for the program stars. The spectral types, magnitudes and colour indices are from the SIMBAD database.

Star	Spectral type	V (mag)	$B-V$ (mag)	N	S/N
HD 23249 (δ Eri)	K0 IV	3.50	0.93	2	350
HD 198149 (η Cep)	K0 IV	3.41	0.94	1	360
HD 222404 (γ Cep)	K1 IV	3.23	1.03	2	320
HD 10780	K0 V	5.63	0.81	2	240
HD 4628	K2 V	5.75	0.88	2	210
HD 201091 (61 Cyg A)	K5 V	5.21	1.18	2	200

2. Observations and data reduction

We have analysed a sample of six stars, whose basic properties are presented in Table 1. The sample is composed of three subgiants (HD 23249, HD 198149 and HD 222404) and three dwarfs (HD 10780, HD 4628 and HD 201091). The sample stars have been selected as stars with low levels of chromospheric activity, i.e. they do not present any evidence of emission (or only little, as in the case of the three dwarfs) in the core of Ca II H and K lines in our spectra. They are bright enough to give a high signal-to-noise ratio and have physical characteristics adequate for testing the reliability of the analysis methods.

The program stars are in the solar neighbourhood ($\lesssim$ 15 pc), are very bright ($V \lesssim 6$) and have modest projected rotational velocities ($v \sin i \lesssim$ 4 km s^{-1}) to limit blends between spectral lines. We assumed that the reddening is negligible within 15 pc.

The spectra were acquired on 2002 November 28 and 29, with the high-resolution cross-dispersed echelle spectrograph SOFIN, mounted on the Cassegrain focus of the 2.56 m Nordic Optical Telescope (NOT) located at the Observatorio del Roque de Los Muchachos (La Palma, Canary Islands). Exposure times ranged from 1 to 20 min, resulting in high S/N ratios per pixel ($\approx$ 0.025 Å/px) averaging at about 280. A spectrum of a Th-Ar lamp was obtained following each stellar spectrum, ensuring accurate wavelength calibration. The spectrograph is equipped with a cross-dispersion prism to separate spectral orders so that many different wavelengths are recorded in a single CCD exposure. The higher the spectral resolution the smaller the part of the spectral range which can be covered by the CCD. The medium resolution optical camera used gives echelle images that contain about 36 orders of ≈ 40 Å each, with increasingly large gaps between redder orders. To circumvent this limitation the observations were carried out in two selected (almost overlapping) settings (#1 and #2) of the echelle and prism angles with limited spectral coverage (except for HD 10780). The change of the spectral setting is done by turning the echelle grating and cross-dispersion prism.

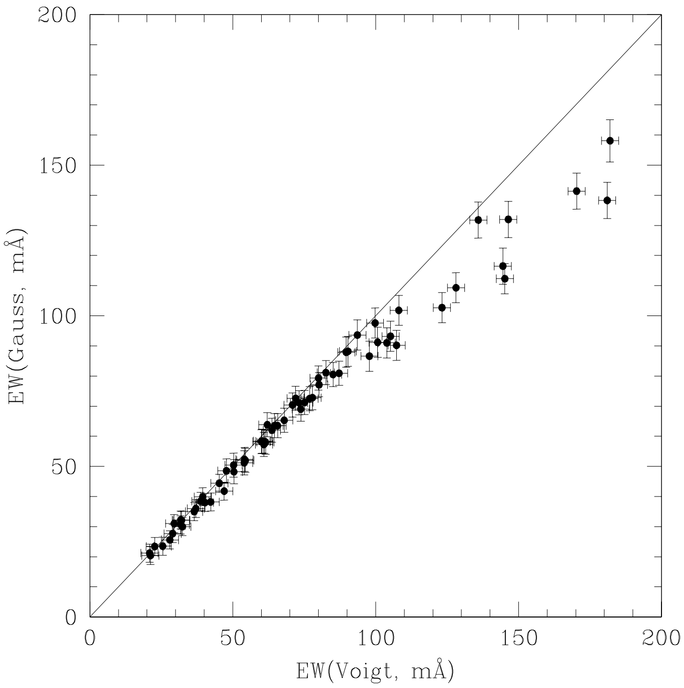

Fig. 1. Comparison of equivalent widths obtained using Gaussian and Voigt profiles for the star δ Eridani (HD 23249). Voigt-profile fitting gives larger values because of the inclusion of the damping wings in the measurements for $EW \geq 100$ mÅ.

The total spectral range is 3900–9900 Å, the resolving power (measured from the Th-Ar emission line spectra) is $R = \lambda/\Delta\lambda \approx 80\,000$. For the dwarf HD 10780 only one setting (#1) was obtained, with the consequence that the spectral coverage for this star is not complete. The spectra were reduced with the standard software available within the CCDRED and ECHELLE packages of IRAF.[1] The analysis includes overscan subtraction, flat-fielding, removal of scattered light, extraction of one-dimensional spectra, wavelength calibration and continuum normalization. Finally, correction for radial velocity shift was applied prior to the measurement of *EW*s. One or two consecutive exposures were generally obtained in order to perform a more robust continuum rectification. For each star we carefully inspected and visually compared the two exposures, in the wavelength intervals which included all the lines used in the abundance analysis, to search for some significant variations between the profiles which could bias the subsequent continuum placement. The two exposures did not show remarkable differences.

We performed the continuum normalization in two steps. We first created a synthetic model atmosphere, using the ATLAS9 code (Kurucz 1993), adopting as atmospheric parameters the average values of previous determinations in the literature and solar metallicity. This model was used to create synthetic spectra for small intervals of 200 to 400 Å to roughly determine the line-free regions, which were fitted by low-degree polynomials using the CONTINUUM task in IRAF. With the detailed spectral analysis of Sect. 3 we obtained more accurate estimates of the atmospheric parameters (mainly of the metallicity) and the procedure described previously was re-iterated.

*EW*s were measured using the SPLOT task in IRAF, assuming a Gaussian profile for weak or moderately strong lines ($EW \lesssim 100$ mÅ) and a Voigt profile for stronger lines. The comparison of these two kinds of measurement (Gaussian and Voigt profiles) for one of the program stars is shown in Fig. 1. As expected, the *EW*s measured by fitting a Voigt function are larger for strong lines than those obtained using Gaussian profiles. Most lines were measured twice on consecutive exposures, and the mean of the measurements was adopted. In these cases the measurements errors are typically not more than a few percent (≈ 3 mÅ). The accuracy (absolute error) is harder to assess; it almost certainly contains a systematic error due to the continuum location, because of the presence of interference fringes (which could not be completely removed) in the redder part of the stellar spectra, which cause a modulation of the local continuum. This error could be particularly important for the weak lines (e.g. for 61 Cyg A).

2.1. Line selection and atomic data calibration

Selection of stellar lines which are free from blends is crucial for deriving accurate elemental abundances. We used, as a starting point, the line list of Morel et al. (2003), which was selected on the basis of a high-resolution spectrum of the K1.5 III star Arcturus (Hinkle et al. 2000). In order to avoid the difficulty in defining the continuum in the blue part of the spectra, only lines with $\lambda > 5500$ Å were selected. Care in the selection of lines is also of importance for the determination of effective temperature by means of excitation equilibrium (which therefore requires that the Fe I lines used cover a wide range in excitation potential). With the exception of iron lines, low-excitation neutral lines, with $\chi < 3.5$ eV (Ruland et al. 1980), were discarded as they are the most affected by NLTE effects. Since we did not have observations of the solar spectrum obtained with the same instrumental configuration as the target stars, we used the same atomic data calibration as Morel et al. (2003). In the present work we adopted $\log\epsilon_{\odot}(\mathrm{Fe}) = 7.67$ instead of the meteoritic value $\log\epsilon_{\odot}(\mathrm{Fe}) = 7.50$ (Grevesse & Sauval 1998), for consistency with Kurucz models and opacities. The analysis performed here is purely differential with respect to the Sun, so this choice has no consequence for our results. The line list of Morel et al. is composed of ≈ 100 lines, 66 of which are present in our final list (we obviously discarded

[1] IRAF (Image Reduction and Analysis Facility) is distributed by National Optical Astronomy Observatories, operated by the Association of Universities for Research in Astronomy, Inc., under cooperative agreement with the National Science Foundation.

lines which fell in the spectral gaps between the spectral orders). Moreover, lines which appeared asymmetric or showed an unusually large width, were assumed to be blended with unidentified lines and therefore discarded from the initial sample. Additional lines, with their log gf values, were taken from Katz et al. (2003) (Fe I λ6861 Å; Fe II λ6432 Å), and Chen et al. (2003) (Fe II λ6247 Å).

The final list of lines as well as the *EW*s used in the abundances analysis are given in Table 6 (only available in electronic form).

3. Data analysis: methods

In order to obtain information on individual abundances from spectral lines of various elements, one must first determine the parameters that characterize the atmospheric model; i.e., the effective temperature, the surface gravity, the microturbulent velocity, and the iron abundance. In principle, these parameters should be determined from the spectrum itself by requiring that measurable quantities (e.g., *EW*s of spectral lines, wing profiles of strong lines, etc.) calculated using the model satisfactorily match the observations. Since these atmospheric parameters are interdependent, an iterative procedure is necessary. The atmospheric parameters ($T_{\rm eff}$, log g, and ξ) and metal abundances were determined using the measured *EW*s and a standard local thermodynamic equilibrium (LTE) analysis with the most recent version of the line abundance code MOOG (Sneden 1973), and a grid of Kurucz (1993) ATLAS9 atmospheres, computed without the overshooting option and with a mixing length to pressure scale height ratio $\alpha = 0.5$. The atmospheres are characterized by an overall metallicity for different chemical species. It is possible to take into account an overabundance of the α-elements with respect to the solar values of 0.2 and 0.4 dex. However, in our study we did not consider this possibility, because all the program stars have α-elements abundance ratios consistent with the solar values. Assumptions made in the models include: the atmosphere is plane-parallel and in hydrostatic equilibrium, the total flux is constant, the source function is described by the Planck function, the populations of different excitation levels and ionization stages are governed by LTE. The abundances are derived from theoretical curves of growth, computed by MOOG, using model atmospheres and atomic data (wavelength, excitation potential, gf values). The input model is constructed using as atmospheric parameters the average values of previous determinations found in the literature, and solar metallicity.

Three different methods were used for the analysis of the sample stars.

Method 1: The photospheric parameters and abundances are obtained by iteratively modifying the effective temperature, surface gravity, micro-turbulence velocity, metallicity and mean α-element abundance of the input model and re-deriving the abundances until (i) the Fe I abundances show no dependence on excitation potential or reduced equivalent width (EW/λ), (ii) the average abundances of Fe I and Fe II are identical (ionization equilibrium) and (iii) the iron and α-elements average abundances are consistent with those of the input model atmosphere.

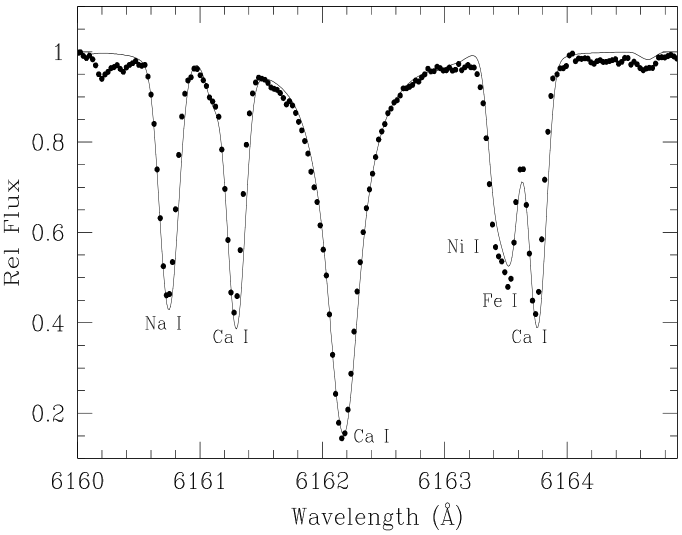

Fig. 2. Comparison between a portion (around Ca I 6162 Å) of the δ Eridani (HD 23249) spectrum (filled dots) and the synthetic profile (solid line).

Method 2: Abundances derived from iron low-excitation lines have been reported to fall systematically below the high-excitation lines in giant stars (Ruland et al. 1980, Drake & Smith 1991, Katz et al. 2003), and this is probably due to non-LTE effects arising from the low density of the photosphere in which they are formed. It is therefore necessary to test whether the results of the first analysis have been affected by non-LTE effects. With this purpose, we have discarded all Fe I lines with $\chi < 3.5$ eV from the initial selection, and this makes it impossible to rely on the slope of the Fe I transition abundances as a function of excitation potential to constrain the atmospheric parameters, as the remaining interval is too limited. In this case, photometric colour indices were used, and the effective temperatures were derived from the $B-V$ index, which has proved to be a more reliable indicator of the stellar effective temperature than the $V-I$ index (Katz et al. 2003). In Table 2 we report the photometric properties of our sample stars and the temperatures derived from the $B-V$ and $V-I$ colours. The colours were converted into effective temperature using the empirical calibration for F0–K5 main sequence stars of Alonso et al. (1996) and for F0–K5 giant stars of Alonso et al. (1999) (for the subgiant stars) using the iron abundance obtained by Method 1. Surface gravities, micro-turbulent velocities and abundances were estimated iteratively in the same way as in the first method, using the restricted set of lines. In the case considered of the $B-V$/temperature transformation, which is metallicity-sensitive, the two steps were iterated until convergence.

Method 3: The third method makes use of information contained in the wings of the 6162 Å Ca I transition. For the sample stars the Ca I line is strong, and therefore its wing profiles are sensitive to surface gravity (Smith, Edvardsson & Frisk 1986; Smith & Drake 1987; Drake & Smith 1991; Zboril & Byrne 1998). The analysis was performed in an iterative way (using as starting parameters those determined with Method 1), since the Ca I wings are also sensitive to the effective temperature,

Table 2. Distance, colour indices (from SIMBAD and Hipparcos Catalogue, ESA 1997), and effective temperatures (we assumed an uncertainty of 100 K for $V-I$ index). The iron abundances reported in this table (from Method 1) were used to derive the effective temperatures from the $B-V$ colour index (Alonso et al. 1996, 1999).

	HD 23249	HD 198149	HD 222404	HD 10780	HD 4628	HD 201091
d (pc)	9	14.3	14	10	8	3.5
$B-V$ (mag)	0.93	0.94	1.03	0.81	0.88	1.18
$(V-I)_c$ (mag)[a]	0.94	0.94	0.99	0.81	0.97	1.13
$(V-I)_J$ (mag)[a]	1.208	1.208	1.272	1.041	1.247	1.452
[Fe/H]	0.05	–0.12	+0.14	–0.10	–0.30	–0.37
$T_{\rm colour}(B-V)$ (K)	4982±180	4889±180	4781±180	5125±160	4876±150	4187±150
$T_{\rm colour}(V-I)$ (K)	4864±100	4751±100	4864±100	5277±100	4867±100	4551±100

[a]: $(V-I)_c$ is measured in the Cousins system, to convert it to the Johnson system used by Alonso et al. (1996, 1999) we used the Bessel (1979) transformation: $(V-I)_J = (V-I)_c/0.778$.

Table 3. Abundance results for the subgiant stars. Number of transitions used to derive the abundances of the different elements (N), mean values (<>) and error bars, corresponding to 1 σ of the atmospheric parameters and abundances, as determined from Methods 1, 2 and 3. The notation is the usual one: $[A/B] = \log[A/B]_\star - \log[A/B]_\odot$.

	HD 23249 (δ Eri)						HD 198149 (η Cep)					
	Method 1		Method 2		Method 3		Method 1		Method 2		Method 3	
	N	<>	N	<>	N	<>	N	<>	N	<>	N	<>
$T_{\rm eff}$ (K)		5140±105		4982±180		5140±50		5080±137		4889±181		5085±80
$\log g$ (cm s^{-2})		4.10±0.26		3.80±0.28		4.10±0.25		3.66±0.22		3.27±0.26		3.68±0.19
ξ (km s^{-1})		1.32±0.18		1.36±0.30		1.25±0.15		1.09±0.10		1.20±0.28		1.13±0.12
$v \sin i$ (km s^{-1})						3.0						3.3
[Fe/H]	38	0.05±0.13	34	–0.05±0.19	34	0.06±0.14	38	–0.12±0.14	34	–0.25±0.19	34	–0.12±0.14
[O/Fe]	3	0.14±0.10	3	0.29±0.12	3	0.09±0.16	3	0.17±0.10	3	0.42±0.12	3	0.17±0.08
[Na/Fe]	1	0.30±0.05	1	0.31±0.12	1	0.29±0.03	1	0.07±0.08	1	0.08±0.11	1	0.07±0.04
[Mg/Fe]	1	–0.10±0.03	1	–0.07±0.11	1	–0.10±0.03	1	–0.05±0.04	1	–0.02±0.11	1	–0.05±0.04
[Al/Fe]	2	0.10±0.03	2	0.14±0.09	1	0.10±0.05	1	0.06±0.08	1	0.08±0.11	1	0.06±0.05
[Si/Fe]	7	0.11±0.09	7	0.19±0.09	7	0.11±0.10	7	0.15±0.20	7	0.24±0.20	7	0.15±0.20
[Ca/Fe]	3	0.08±0.14	3	0.08±0.15	3	0.10±0.14	3	0.08±0.13	3	0.06±0.23	3	0.09±0.10
[Sc/Fe]	1	0.25±0.12	1	0.16±0.19	1	0.24±0.14	1	0.10±0.15	1	0.01±0.18	1	0.10±0.08
[Ti/Fe]	1	0.07±0.07	1	0.05±0.17	1	0.07±0.05	1	–0.05±0.11	1	–0.07±0.14	1	–0.05±0.06
[Cr/Fe]	2	–0.02±0.13	2	–0.03±0.12	1	–0.01±0.16	1	–0.07±0.10	1	–0.10±0.20	1	–0.06±0.08
[Co/Fe]	1	0.16±0.10	1	0.13±0.18	1	0.16±0.12	1	0.16±0.10	1	0.12±0.17	1	0.17±0.07
[Ni/Fe]	5	0.07±0.14	5	0.08±0.15	5	0.08±0.17	5	0.02±0.12	5	0.02±0.17	5	0.03±0.11
[Ba/Fe]	1	–0.06±0.24	1	–0.20±0.19	1	–0.02±0.26	1	0.05±0.21	1	–0.15±0.18	1	0.05±0.15
[α/Fe]		0.04±0.05						0.03±0.07				

micro-turbulent velocity and calcium abundance. Before applying the method we made a detailed comparison between the observed profile of the 6455 Å Ca I line and a synthetic profile calculated using the *synth* task in MOOG, with the atmospheric parameters determined with Method 1. This line is less sensitive to variations of the surface gravity than the 6162 Å Ca I line. The calculated profile was broadened by a Gaussian distribution with full width at half maximum ($FWHM$) ≈ 0.08 Å, to make appropriate allowance for the instrumental profile (which was obtained measuring a Th-Ar emission line). A comparison of this kind has been made to measure the value of the projected rotational velocity[2] ($v \sin i$), that gives the best agreement between the calculated profile and the observed one.

[2] The $v \sin i$ value determined in this way simultaneously accounts for the effect of stellar rotation and macroturbulence.

Derived $v \sin i$ values are reported in Table 3 and 4. For the 6162 Å line we used a van der Waals damping based on both the classical Unsold approximation and the enhanced Unsold approximation multiplied by a factor (option 2 in the damping parameter in MOOG). The comparison of the stellar parameters obtained in the two cases reveals that the surface gravities derived using the enhancement factor are lower by 0.17 dex at most. However, for both the effective temperatures and metallicities the differences are very small, not exceeding 20 K and 0.03 dex, respectively.

For this method the analysis proceeds in two steps for each star. In a first step, the surface gravity is derived by comparing the observed 6162 Å Ca I wing profiles to a synthetic profile (Fig. 2) created using the atmospheric parameters obtained in Method 1 and the value of $v \sin i$ determined previously from the 6455 Å line. The comparison proceeds until the two pro-

Table 3. Continued.

	HD 222404 (γ Cep)					
	Method 1		Method 2		Method 3	
	N	<>	N	<>	N	<>
$T_{\rm eff}$ (K)		4935±139		4781±179		5020±115
log g (cm s^{-2})		3.63±0.38		3.22±0.42		3.85±0.27
ξ (km s^{-1})		1.41±0.17		1.56±0.26		1.26±0.17
$v \sin i$ (km s^{-1})						3.0
[Fe/H]	38	0.14±0.19	34	0.01±0.23	34	0.22±0.25
[O/Fe]	3	0.04±0.31	3	0.24±0.30	3	–0.06±0.15
[Na/Fe]	1	0.06±0.08	1	0.09±0.13	1	0.05±0.07
[Mg/Fe]	1	–0.03±0.05	1	0.02±0.12	1	–0.06±0.06
[Al/Fe]	1	0.12±0.09	1	0.14±0.15	1	0.10±0.12
[Si/Fe]	7	0.10±0.20	7	0.19±0.20	7	0.05±0.09
[Ca/Fe]	3	–0.09±0.18	3	–0.13±0.29	3	–0.06±0.15
[Sc/Fe]	1	0.40±0.24	1	0.32±0.27	1	0.45±0.26
[Ti/Fe]	1	–0.02±0.12	1	–0.03±0.18	1	–0.02±0.14
[Cr/Fe]	1	–0.08±0.15	1	–0.12±0.27	1	–0.04±0.11
[Co/Fe]	1	0.31±0.17	1	0.28±0.23	1	0.35±0.19
[Ni/Fe]	5	–0.02±0.18	5	–0.03±0.22	5	0.00±0.15
[Ba/Fe]	1	–0.30±0.27	1	–0.51±0.54	1	–0.13±0.17
[α/Fe]		–0.01±0.07				

files are in good agreement, and the surface gravity value is that used to create the model atmosphere. In a second step, the measured equivalent widths of the set of lines used in Method 2 are converted to abundances, as in the first two methods. The surface gravity of the MOOG input atmospheric model is the one derived during the first step. In this case we used the ionization equilibrium to determine the effective temperature, since we discarded the low excitation potential lines from the line list. Effective temperature, surface gravity, micro-turbulence velocity and abundances are obtained modifying the input $T_{\rm eff}$, ξ, [Fe/H] and [Ca/H] values and repeating the two steps until (i) the Fe I transitions exhibit no trend with EW/λ, (ii) the Fe I and Fe II lines give the same average abundances and (iii) the iron and calcium average abundances are consistent with the input abundances.

3.1. Error determination

There are two kinds of uncertainties in the determination of atmospheric parameters and abundance: the first acts on individual lines, and includes random errors of equivalent widths; the second acts on the whole set of lines with the main uncertainties coming from the errors inherent in the different diagnostics used to determine the three parameters (excitation and ionization equilibria of the iron lines to determine $T_{\rm eff}$ and $\log g$; the independence of the abundances given by the Fe I lines as a function of EW/λ, to determine ξ). The errors were derived in several steps.

1. We first calculate the $1\,\sigma$ errors in each of the individual diagnostics. We vary the temperature value until the slope of the Fe I abundances vs excitation potential graph differs from zero at the $1\,\sigma$ level; similarly, we vary the microturbulence value until the slope of the Fe I abundances vs W/λ graph differs from zero at the $1\,\sigma$ level; keeping the $T_{\rm eff}$ value fixed we vary the $\log g$ value until the abundances of Fe I and Fe II lines show a difference of $1\,\sigma$. The uncertainties in the atmospheric parameters due to each individual diagnostic have been quadratically summed. The correlation of the errors in temperature and gravity is specially important for gravity. The gravity error was computed according to Eq.(1) below (analogous equations were used to compute the $T_{\rm eff}$ and ξ errors):
$$\sigma(\log g)^2 = [\partial(\log g)/\partial(\mathrm{Fe\,I,Fe\,II})\cdot\sigma(\mathrm{Fe\,I,Fe\,II})]^2 + [\partial(\log g)/\partial(T_{\rm eff})\cdot\sigma(T_{\rm eff})]^2 + [\partial(\log g)/\partial(\xi)\cdot\sigma(\xi)]^2. \quad (1)$$
2. The three parameters of the atmospheric models were varied, one by one, by the relevant uncertainty, and the effect on the mean abundance of each element derived. The differences between the convergent models and the models obtained considering the uncertainties in each of the individual diagnostics (one at a time) give the final errors in the three parameters.
3. The 3 individual errors in the mean abundance of each element, calculated in this way, were quadratically summed with the uncertainty due to the line-to-line scatter in the abundance determinations.

For an elemental abundance derived from many lines the uncertainty of the atmospheric parameters is the dominant error, while for an abundance derived from a few lines, the uncertainty in the equivalent widths may be more significant. The analysis for some elements (Na, Mg, Ti and Ba) relies on a single line lying on the flat portion of the curve of growth, therefore the derived abundances should be treated with some caution.

The uncertainty in $T_{\rm eff}$ for Method 2 is obtained from the empirical calibration of Alonso et al. (1996) and Alonso et al.

Table 4. Mean values of the derived atmospheric parameters and abundances for the dwarf stars as determined from Methods 1 and 2 (<>). Blanks indicate that the equivalent widths could not be reliably measured.

	HD 10780				HD 4628				HD 201091 (61 Cyg)	
	Method 1		Method 2		Method 1		Method 2		Method 1[b]	
	N	<>	N	<>	N	<>	N	<>	N	<>
$T_{\rm eff}$ (K)		5300± 95		5125±158		5080±130		4876±150		4525±140
log g (cm s^{-2})		4.13±0.23		3.79±0.35		4.59±0.26		4.12±0.28		4.65±0.25
ξ (km s^{-1})		1.17±0.29		1.41±0.32		1.06±0.24		1.36±0.31		1.34±0.24
$v \sin i$ (km s^{-1})				0.6 [a]				1.7		1.1
[Fe/H]	25	–0.10±0.10	22	–0.22±0.14	36	–0.30±0.15	32	–0.42±0.18	26	–0.37±0.19
[O/Fe]	3	0.13±0.09	3	0.34±0.12	2	0.27±0.23	2	0.51±0.22		
[Na/Fe]					1	0.04±0.06	1	0.05±0.08	1	0.10±0.06
[Mg/Fe]					1	0.31±0.04	1	0.42±0.02	1	0.02±0.04
[Al/Fe]					2	0.26±0.07	2	0.21±0.06	2	0.10±0.11
[Si/Fe]	3	–0.01±0.07	7	0.05±0.10	5	0.02±0.15	5	0.13±0.15	3	0.07±0.12
[Ca/Fe]	1	0.08±0.12	1	0.03±0.26	3	0.05±0.10	3	0.03±0.18	3	0.05±0.10
[Sc/Fe]										
[Ti/Fe]	1	–0.02±0.07	1	–0.03±0.12	1	–0.06±0.11	1	0.03±0.13	1	0.12±0.11
[Cr/Fe]	1	0.08±0.10	1	0.04±0.15	2	0.03±0.10	2	–0.02±0.18	2	0.20±0.10
[Co/Fe]	1	0.03±0.08	1	0.01±0.12	1	0.03±0.09	1	–0.01±0.12		
[Ni/Fe]	3	0.00±0.11	3	–0.02±0.15	4	–0.06±0.12	4	–0.05±0.16	5	–0.10±0.12
[Ba/Fe]					1	–0.25±0.31	1	–0.49±0.44	1	–0.35±0.30
[α/Fe]		0.02±0.05				0.08±0.05				0.04±0.05

[a]: From Fekel (1997).
[b]: Although the approach adopted for the analysis of 61 Cyg A (described in Sect. 4.1) is completely different from the first one, we maintain the notation "Method 1". We consider the atmospheric parameters ($T_{\rm eff}$ and ξ) obtained in this way, together with the temperature derived from the $B-V$ index, which is metallicity-sensitive, as approximate estimates.

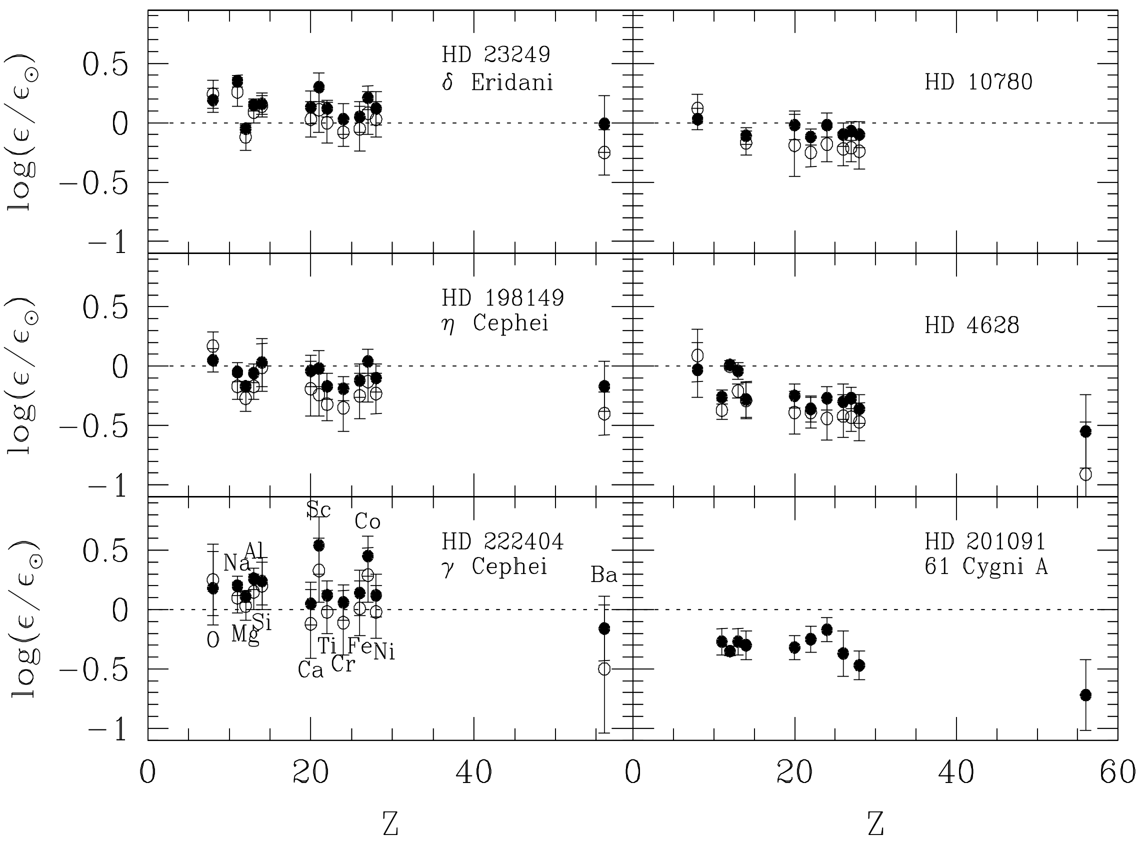

Fig. 3. Abundance patterns for the program stars, determined from Method 1 (filled circles) and Method 2 (open circles).

(1999) as the quadratic sum of 4 individual 1 σ errors: (1) the uncertainty due to internal errors in the calibration; (2) the intrinsic uncertainty of the photometry, typically 0.03 mag (15 K per 0.01 mag for $B-V > 0.8$, for giant stars; 50 K per 0.01 mag for $B-V > 0.6$, for dwarf stars); (3) the uncertainty obtained by inserting the metallicity error in the empirical calibration; (4) the uncertainty of 150 K reflecting the intrinsic scatter between the various colour-$T_{\rm eff}$ empirical calibrations in the literature.

To estimate the uncertainties in *logg* for Method 3 we synthesized the spectra around the 6162 Å feature with different *logg* values, and estimated (by eye) the maximum variation of gravity consistent with the observed spectra.

4. Results and discussion

4.1. Abundances and atmospheric parameters

The atmospheric parameters and abundances derived for the sample stars, with the three methods outlined in Sect. 3, are presented in Table 3 and 4. Having applied the three different techniques to our 6 program stars, we have successfully obtained converging solutions for each of the parameters in almost all cases. The abundances derived from the Fe I and Fe II lines are consistent.

We note, as a general trend, that the effective temperatures and surface gravities obtained with Method 2 are systematically lower than those obtained with Method 1, with maximum differences of 200 K for $T_{\rm eff}$ and 0.47 dex for $\log g$ (for 61 Cyg A we found a difference of ≈ 340 K between the spectroscopic temperature and that derived from the $B-V$ colour index, see discussion below). Nevertheless, the differences obtained influence only the abundance of [O/Fe] (up to 0.25 dex) and [Ba/Fe] (up to 0.24 dex). For Fe and the other elements the results given by the first two methods are discrepant by 0.13 dex at most. The abundance ratios of the chemical elements obtained with Methods 1 and 2 show the same global pattern (Fig. 3) and are compatible within the uncertainties. In some cases (e.g., Ba), the differences are largely due to the small number of lines used in the analysis. The atmospheric parameters and abundances derived from Method 3, for the three subgiant stars, are in fairly good agreement with those obtained from Method 1.

The analysis of HD 201091 (61 Cygni A), which is the coolest star of the sample, has been problematic, for the following reasons:

1. at this low temperature the *EW*s are not easily measured because the spectra are severely affected by blending with molecular bands;
2. blending was also severe for the few weak ($\lesssim 10$ mÅ) Fe II lines, which we did not measure.

The lack of the Fe II *EW*s made it impossible to rely on the ionization equilibrium to determine the surface gravity with Methods 1 and 2, and the effective temperature with Method 3. Nevertheless, we have performed the analysis for this star with Method 1, testing the gravity values, by steps of 0.5 dex, in the interval $4.30 \lesssim \log g \lesssim 4.90$ of previous determinations found in the literature. With $\log g = 4.65$ we obtained a convergent (but not self-consistent) solution. The atmospheric parameters, ($T_{\rm eff}$ and ξ) and the abundances obtained are shown in Table 4.

The application of Method 3 to the dwarfs of the sample did not lead to convergent solutions, though it works very well for subgiants. The application of the analysis to HD 10780 was not performed because the Ca I line is not included in the single setting (#1) obtained for this star. For the other dwarf star (HD 4628, of spectral type K2) for which this kind of analysis was possible we did not find a convergent solution. The determination of ξ failed; i.e., the solution eventually goes to (unphysical) negative values, which may indicate that the assumption of depth-independent microturbulence is not adequate for modeling the atmosphere of such late dwarfs (Takeda et al. 2002). We performed several tests in order to obtain a convergent solution with Method 3 (and to identify the possible source of the problem):

1. gravities from the theoretical isochrones were used in the analysis instead of those obtained from the Ca I line fitting;
2. the Ca abundance was varied, to take into account a possible wrong abundance determination which is based, for Ca, on 3 lines, two of which are strong;
3. the analysis was repeated discarding very strong Fe I lines ($EW \geq 100$ mÅ) to avoid systematic errors in the *EW* measurements and uncertainties in the damping parameters.

None of these tests led to a convergent solution with Method 3 for HD 4628, at variance with Method 1 which led to convergent solutions for all the sample stars (with the exception of the coolest star, discussed above).

The derived abundances for the program stars with the three methods are consistent with the solar values, with some exceptions. Sc, O and Co exhibit a slight overabundance in some of the sample stars, as is the case for Na in δ Eri and Mg and Al in HD 4628. However, the abundances obtained show the typical trend with metallicity of disk stars (Reddy et al. 2003; Chen et al. 2003). The α-elements (defined as the mean of the Mg, Si, Ca, and Ti abundances) have abundance ratios consistent with the solar values for all the sample stars.

4.2. Comparison with previous works

The sample stars have been previously analysed in the literature. Despite adopting different approaches and different log gf values, the agreement of this work with Santos et al. (2001) for HD 23249 (δ Eri) and with Feltzing & Gonzalez (2001) for HD 10780 is quite satisfactory for $T_{\rm eff}$, $\log g$, and for almost all the elements. For HD 10780, the largest deviation is 0.12 dex in [Ti/Fe], which can be explained by the small number of lines used in the analysis for this element (1 line used in this work and 2 lines used in the work of Feltzing & Gonzalez). Chen et al. (2003) analysed the star HD 10780 but used the Hipparcos-parallax-derived gravity which is significantly higher ($\log g = 4.49$) than the spectroscopic value of Feltzing & Gonzalez (2001) and of the present work ($\log g = 4.13$). Our relative abundances and those of Chen et al. are, however, consistent with a maximum deviation of 0.08 dex for [Fe/H].

Mashonkina et al. (2001) found HD 198149 (η Cep) to have [Fe/H] = −0.14 and [Ba/Fe] = 0.04, using a spectrum

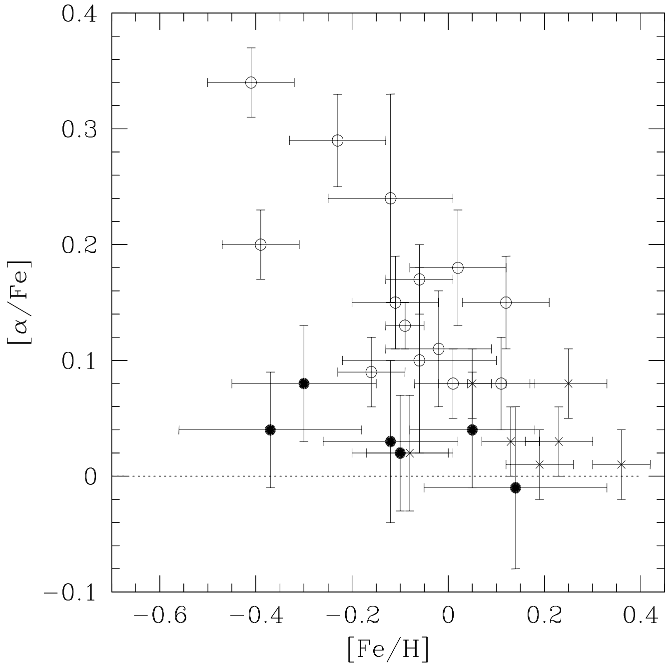

Fig. 4. Comparison between the abundance ratio of the α-synthesized elements as a function of [Fe/H] obtained from Method 1 (filled circles) for the stars in our sample and those obtained by Morel et al. (2003, 2004) with a similar approach, for a different sample of stars: active binaries (open circles) and inactive (presumably single) control stars (crosses) of similar spectral types (late G- to early-K subgiants).

with nearly half the resolution of ours. Nevertheless, they are in good agreement with our −0.12 and 0.05 values, derived using 33 and 1 lines, respectively.

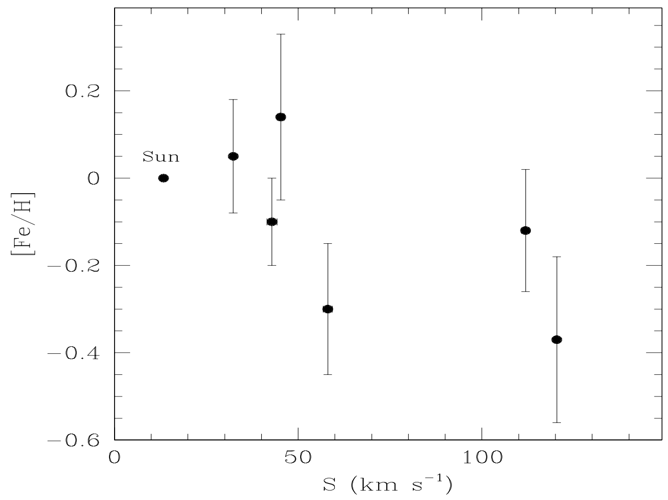

Fig. 5. [Fe/H] as a function of peculiar space velocities for Method 1 for the stars in our sample.

For HD 4628 and HD 201091 (61 Cyg A) Zboril & Byrne (1998) found [Fe/H] = −0.27 and −0.3, respectively; our estimate of [Fe/H] for HD 4628 is −0.3, which is in excellent agreement with previous work. Our estimate of [Fe/H] for HD 201091 is −0.37; however, Methods 2 and 3 do not converge for this star, so nothing definitive can be said about this result. These different comparisons give us confidence that our analysis is satisfactory.

We have compared our abundances of the α-synthesized elements (Method 1) with those obtained, for a different sample of stars, by Morel et al. (2003, 2004). They carried out an analysis, similar to the present one, of 14 single-lined active binaries and of a control sample made up of 7 single (inactive) stars of similar spectral types (late G- to early-K subgiants). The three samples differ slightly in the metallicity values, as can be seen in Fig. 4, and, mainly, in the activity levels: the active binary stars have relatively "low" metallicity and high activity; the control sample stars have relatively "high" metallicity and low activity, and the stars of the present work, which cover the entire temperature and metallicity range of the other two samples, have low activity. There is a good agreement between the abundance patterns of our sample and the control sample of Morel et al., which are both at variance with that of the sample with low-metallicity/high-activity (active binaries). Active binaries show a relative overabundance of the α elements compared to the two other (non-active) samples. The stars analysed by Morel et al. (including the control sample) cover age and mass intervals which almost overlap those covered by our sample; therefore, beyond a possible explanation in the framework of standard evolutionary theory, it seems that the peculiar abundance pattern found in active binaries can be mainly related to the different activity levels (see also Morel & Micela 2004).

4.3. Stellar kinematics

Stars presently near the Sun may come from a wide range of Galactic locations. Information on their origin will help us to understand their abundance ratios. Therefore, stellar space velocity, as a clue to the origin of a star in the Galaxy, is very important. The accurate distance and proper motion available in the Hipparcos Catalogue (ESA, 1997), combined with the stellar radial velocity, make it possible to derive reliable space velocities for our program stars. The calculation of the space velocity with respect to the Sun is based on the procedure presented by Johnson & Soderblom (1987), corrected for the effect of differential galactic rotation (Scheffler & Elsässer 1988), by adopting a solar Galactocentric distance of 8.5 kpc and a circular velocity of 220 km s^{-1}. The correction of space velocity to the Local Standard of Rest is based on a solar motion[3], $(U, V, W)_{\odot} = (10.0, 5.2, 7.2)$ km s^{-1}, as derived from Hipparcos data by Dehnen & Binney (1998). The peculiar space velocity S, given by $S = (U^2 + V^2 + W^2)^{1/2}$, is quoted with all kinematic data in Table 5 and is shown as a function of [Fe/H] in Fig. 5. As can be seen, HD 23249, HD 222404, HD 10780 and HD 4628 show kinematic (and chemical) properties typical of the thin disk population, while HD 198149, and HD 201091 show one velocity component which suggests a thick disk or halo origin (Soubiran 1993). We have calculated the probabilities that the sample stars belong to a specific population, thick (TD), thin disk (D) or stellar halo (H), following the method used by Bensby, Feltzing & Lundström (2004). On account of

[3] In the present work, $\boldsymbol{U}$ is defined to be positive in the direction of the Galactic center.

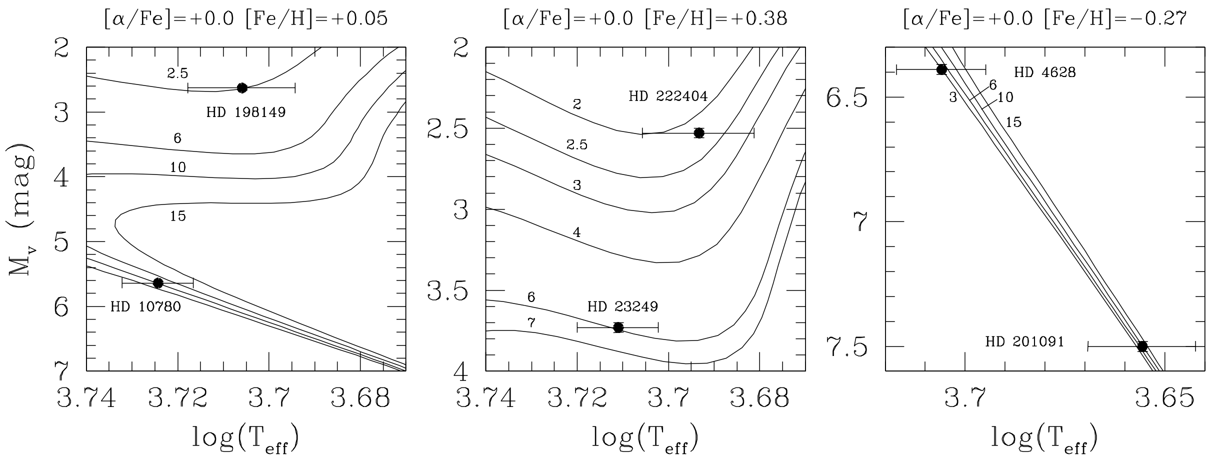

Fig. 6. Diagrams used to estimate ages for our program stars (Method 1). The theoretical isochrones are taken from Yi et al. (2003). The metallicities of the isochrones refer to a solar iron abundance: $\log \epsilon_{\odot}$(Fe)=7.50 (Yi et al. 2001, 2003; Kim et al. 2002). The isochrones are shown for [α/Fe]=0.0 and [Fe/H]=0.05 (*left-hand panel*), [α/Fe]=0.0 and [Fe/H]=+0.38 (*middle panel*), and [α/Fe]=0.0 and [Fe/H]=−0.27 (*right-hand panel*). The ages of the isochrones (in Gyr) are indicated in every panel.

these probabilities, HD 198149 and HD 201091 could belong to the thick disk, because their ratios of the respective probabilities for the thin and thick disks are $D/TD \lesssim 0.5$ (Bensby et al. 2004). The other stars of the sample display probability ratios typical of the thin disk, while none seems to belong to the halo.

4.4. Evolutionary status

Stellar age is a fundamental parameter when studying the chemical evolution of the Galaxy as a function of time. The available Hipparcos parallaxes have provided distances to many stars in the solar neighborhood, and these measurements allow us to constrain the stellar gravities by comparison with stellar models. In this section, the gravities from the theoretical isochrones are compared with the gravities obtained spectroscopically from the neutral and ionized iron lines. We determined the positions of the sample stars in the H-R diagram for the appropriate Fe and [α/Fe] abundances, using $T_{\rm eff}$ obtained with Method 1 and the absolute magnitudes, $M_{\rm v}$, derived from Hipparcos parallaxes, and they are plotted in Fig. 6, together with the isochrones, derived for scaled-solar mixture, of Yi et al. (2003). The correct isochrones were chosen depending on the [Fe/H] for each star as derived in this work (Method 1), making appropriate corrections for the different solar iron abundances assumed. The three subgiants (HD 23249, HD 198149, HD 222404) are all starting to ascend the red giant branch, and have evolved from main-sequence stars with masses ranging from about 1.2 to 1.7 $M_{\odot}$, as suggested by the stellar masses obtained from the evolutionary tracks (Table 5). Fig. 7 shows the comparison between the gravities derived from the ionization equilibrium of the Fe lines and from the evolutionary tracks. A reasonable agreement is found, although the three subgiant stars show values of spectroscopic gravity systematically higher than those derived from the evolutionary tracks. A possible explanation for the anomalously low value of the gravity derived from the ionization equilibrium for the dwarf star HD 10780 may be attributed to the insufficient number of iron lines on which the analysis is based for this star.

5. Conclusions

We have presented a detailed abundance analysis of six K-type dwarf and subgiant stars, with the use of three different techniques, which have been compared in order to establish their respective merits and faults, aiming at deriving, in the near future, the chemical composition of larger samples of nearby K-type stars with a self-consistent and reliable method.

These techniques rely on: (i) the excitation and ionization equilibrium of the Fe I and Fe II lines to determine the effective temperature and the surface gravity; (ii) the color-index/temperature transformation; and (iii) the detailed fitting of the wings of collisionally-broadened lines to determine the surface gravity.

Methods 1 and 3 give consistent results for our program stars; in particular, the results obtained suggest that the Fe I low excitation potential transitions do not appear significantly affected by non-LTE effects, and, as a consequence, the iron excitation equilibrium is a reliable diagnostic in the analysed stars. The first method appears to be the most reliable, as it is self-consistent and yields results that are in good agreement with the previous determinations in the literature. The solutions of the parameters were confirmed to successfully converge for all the sample stars (early and late type), except in one case (the coolest star). This suggests that spectral type K5 V represents, with our methods, about the limit for useful equivalent width work at these wavelengths. In fact, in these cases, blends with molecular bands and the weakness of the lines of some elements are severe constraints on their abundance determinations; lines in the visual spectral region can be measured with comparative ease for type K0 V and earlier, but the accuracy begins to fall off towards later spectral types, so a different approach must be sought for analysing stars with effective temperatures less than 4500 K. The second method is not self-consistent and, moreover, leads to effective tempera-

Table 5. Kinematic data and age determinations ($\tau_{\rm iso}$). The top half of the table contains information about coordinates (from the Hipparcos Catalogue, ESA 1997), and radial velocities of the program stars (from the SIMBAD database). All coordinates used are for equinox 1950. The lower section shows the velocity data obtained, along with evolutionary ages. The last row gives the stellar mass derived from the evolutionary tracks (Method 1).

	HD 23249	HD 198149	HD 222404	HD 10780	HD 4628	HD 201091
l (°)	198.09	97.87	118.99	129.09	121.51	82.32
b (°)	–46.00	11.64	15.32	1.66	–57.58	–5.82
π (mas)	110.58±0.88	69.73±0.49	72.50±0.52	100.24±0.68	134.04±0.86	287.13±1.51
$\mu_\alpha \cos\delta$ (mas)	–91.71±0.98	86.08±0.44	–48.85±0.48	582.05±0.43	758.04±0.73	4155.10±0.95
μ_δ (mas)	742.23±0.92	817.89±0.39	127.18±0.44	–246.83±0.55	–1141.22±0.57	3258.90±1.19
v_r (km s^{-1})	–6.1±0.9	–87.3±0.9	–42.4±0.9	2.8±2.0	–12.6±2.0	–64.3±0.9
U (km s^{-1})	–23.5±0.7	–45.1±0.5	11.3±0.6	–34.9±1.3	–10.5±0.7	–104.1±0.6
V (km s^{-1})	21.5±0.7	–102.3±1.1	–42.7±1.0	–21.5±1.7	–54.0±1.1	–58.5±1.1
W (km s^{-1})	5.7±0.8	3.8±0.5	–9.8±0.5	–12.7±0.4	–18.5±1.7	–15.2±0.4
S (km s^{-1})	32.4±0.7	111.9±1.0	45.3±0.9	42.9±1.4	58.1±1.2	120.4±0.7
$\tau_{\rm iso}$ (Gyr)	6±1	2.5±0.3	2.2±0.2	6±4	3±1.5	10^{+5}_{-6}
M (M$_\odot$)	1.2	1.6	1.7	0.9	0.8	0.6

tures, and consequently surface gravities, systematically lower than those obtained with the other two. This behaviour could be attributed to residual non-LTE effects in Method 1 (although not confirmed by the results of Method 3) or may be due to a colour-$T_{\rm eff}$ scale biased towards cooler temperatures; the use of different colour indices and calibration scales gives $T_{\rm eff}$ values which are in some cases slightly higher and in some cases slightly lower than those found with Alonso's calibration. To firmly assess this point it would be useful to analyse a larger sample of K-stars.

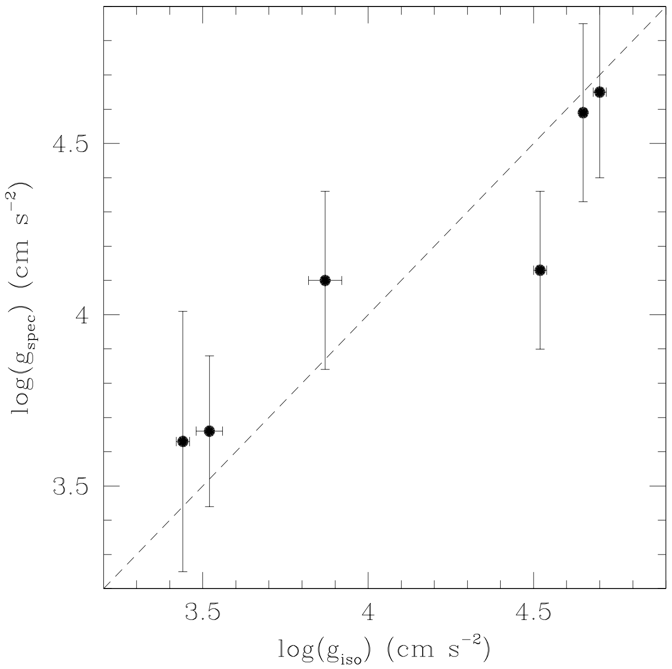

Fig. 7. Comparison of the gravities derived by Method 1 with the values given by the theoretical isochrones. The error bars for the theoretical gravities were derived from the uncertainties in the position of the stars in the HR diagrams.

Method 3, which is self-consistent and like Method 2 does not use Fe I low excitation potential transitions, gives results that are in good agreement with Method 1, again confirming the absence of supposed departures from LTE (at least for the three subgiant stars of the sample, for which the analysis has led to convergent solutions). The application of Method 3 to the dwarfs did not lead to convergent solutions. The problem could be connected to some of the assumptions involved in the adopted models for such late-type dwarfs. Although we cannot specify which element of our method causes a problem with the analysis of dwarf stars (we recall that using the Hipparcos gravities, varying the Ca abundance and discarding strong lines from the analysis was of no help), further study of late K-type dwarfs will help clarify the source of this problem.

Because of the good agreement between our results and those obtained from other works, we are confident that the analysis methods employed lead to robust results and, consequently, can be extended to a larger sample of stars.

Comparison with a sample of active binary stars (Morel et al. 2004) using a similar analysis shows a different behaviour of the α-elements: at variance with that work, which shows an overabundance of the α-elements, here we find abundance ratios consistent with the solar values for all the program stars, in good agreement with the abundance pattern obtained by Morel et al. for their control sample of inactive stars.

The analysis methods tested in the present work have led to robust results and, in particular, the two self-consistent methods (with the appropriate improvements to account for cooler and later type stars) constitute a reliable means for the detailed analysis of disk stars abundance ratios (down to ≈ K5), that are key population indicators and will allow us to quantitatively study models of the chemical evolution of the Galaxy.

Acknowledgements. We wish to thank the referee R. D. Jeffries for several helpful suggestions which have been incorporated in the manuscript. T. M and J. S. acknowledge support by the Marie Curie Fellowship Contract No. HPMD-CT-2000-00013. This research has made use of the SIMBAD database, operated at CDS, Strasbourg, France, and of NASA's Astrophysics Data System Abstract Service.

References

Alonso, A., Arribas, S., & Martínez-Roger, C. 1996, A&A, 313, 873
Alonso, A., Arribas, S., & Martínez-Roger, C. 1999, A&AS, 140, 261
Bensby, T., Feltzing, S., & Lundström, I. 2004, A&A, 415, 155
Bessell, M. S. 1979, PASP, 91, 589
Castelli, F. & Hack, M. 1990, Mem. SAIt, 61, 595
Chen, Y. Q., Nissen, P. E., Zhao, G., Zhang, H. W., & Benoni, T. 2000, A&AS, 141, 491
Chen, Y. Q., Zhao, G., Nissen, P. E., Bai, G. S., & Qiu, H. M. 2003, ApJ, 591, 925
Dehnen, W., & Binney, J. J. 1998, MNRAS 298, 387
Drake, J. J. 1991, MNRAS, 251, 369
Edvardsson, B. 1988, A&A, 190, 148
ESA, 1997, The Hipparcos and Thyco catalogues, ESA SP-1200
Favata, F., Micela, G., Sciortino, S., & Morale, F. 1997, A&A, 324, 998
Fekel, F. C. 1997, PASP, 109, 514
Feltzing, S. & Gustafsson, B. 1998, A&AS, 129, 237
Feltzing, S. & Gonzalez, G. 2001, A&A, 367, 253
Fuhrmann, K. 1998, A&A, 338, 161
Gray, D. F. 1994, PASP, 106, 1248
Grevesse, N., Noels, A., & Sauval, A. J. 1993, A&AS, 271, 587
Grevesse, N. & Sauval, A. J. 1999, A&A, 347, 348
Hinkle, K., Wallace, L., Valenti, J., & Harmer, D. 2000, Visible and Near Infrared Atlas of the Arcturus Spectrum 3727-9300 Å, (San Francisco: ASP)
Johnson, D. R. H., & Soderblom, D. R. 1987, AJ, 93, 864
Katz, D., Favata, F., Aigrain, S., & Micela, G. 2003, A&A, 397, 747
Kim, Y.-C., Demarque, P., Yi, S. K., & Alexander, D. R. 2002, ApJS, 143, 499
Kurucz, R. L. 1993, ATLAS9 Stellar Atmosphere Programs and 2 km/s grid. Kurucz CD-ROM No. 13. Cambridge, Mass.: Smithsonian Astrophysical Observatory, 1993, 13
Mashonkina, L. & Gehren, T. 2001, A&A, 376, 232
Morel, T., Micela, G., Favata, F., Katz, D., & Pillitteri, I. 2003, A&A, 412, 495
Morel, T., Micela, G., Favata, F., & Katz, D., 2004 A&A, in press (astro-ph/0406348)
Morel, T., & Micela, G., 2004, A&A, 423, 677
Reddy, B. E., Tomkin, J., Lambert, D. L., & Allende Prieto, C. 2003, MNRAS, 340, 304
Ruland, F., Holweger, H., Griffin, R., Griffin, R., & Biehl, D. 1980, A&A, 92, 70
Santos, N. C., Israelian, G., & Mayor, M. 2001, A&A, 373, 1019
Scheffler, H., & Elsässer, H. 1988, in Physics of the Galaxy and Interstellar Matter (Springer Verlag: Berlin)
Smith, G., Edvardsson, B., & Frisk, U. 1986, A&A, 165, 126
Smith, G. & Drake, J. J. 1987, A&A, 181, 103
Sneden, C. A. 1973, Ph.D. Thesis University of Texas, Austin
Soubiran, C. 1993, A&A, 274, 181
Takeda, Y., Sato, B., Kambe, E., Sadakane, K., & Ohkubo,M. 2002, PASJ, 54, 1041
Yi, S., Demarque, P., Kim, Y., Lee, Y., Ree, C. H., Lejeune,T., & Barnes, S. 2001, ApJS, 136, 417
Yi, S. K., Kim, Y., & Demarque, P. 2003, ApJS, 144, 259
Wyse, R. F. C. 1998, ASP Conf. Ser. 142: The Stellar Initial Mass Function (38th Herstmonceux Conference) edited by Gary Gilmore and Debbie Howell. ASP Conference Series, Vol. 142, 1998, 89
Zboril, M. & Byrne, P. B. 1998, MNRAS, 299, 753

Table 6. Wavelengths, excitation potentials and log gf values from Morel et al. (2003), and equivalent widths measured in the program stars.

λ (Å)	χ (eV)	log gf	EW (mÅ)[a]					
			δ Eri	η Cep	γ Cep	HD 10780	HD 4628	61 Cyg
O I; log $\epsilon_{\odot}$(O)=8.93								
7771.944	9.147	0.297	44.4	44.4	28.8	49.5	24.3	
7774.166	9.147	0.114	35.0	34.5	33.5	36.4	27.5	
7775.388	9.147	–0.064	27.7	26.7	33.7	34.5		
Na I; log $\epsilon_{\odot}$(Na)=6.33								
6154.226	2.102	–1.637	87.9	56.0	84.2		47.6	81.1
Mg I; log $\epsilon_{\odot}$(Mg)=7.49								
5711.088	4.346	–1.514	135.9	120.8	152.0		172.9	132.7
Al I; log $\epsilon_{\odot}$(Al)=6.47								
6698.673	3.143	–1.843	51.2	37.0	64.1		37.4	44.3
7835.309	4.022	–0.663	72.5				56.0	61.0
Si I; log $\epsilon_{\odot}$(Si)=7.55								
5793.073	4.930	–1.894	58.0	49.0	63.2	41.7	38.8	24.8
5948.541	5.083	–1.098	107.3	115.4	120.9	87.3	64.6	46.2
6155.134	5.620	–0.742	93.6	74.4	81.5		55.4	31.1
6721.848	5.863	–1.100	58.3	41.8	67.9			
7034.901	5.871	–0.779	69.0	60.0	66.9	62.1	38.0	
7760.628	6.206	–1.356	23.4	30.8	30.5			
8742.446	5.871	–0.448	91.0	84.5	88.8		87.3	
Ca I; log $\epsilon_{\odot}$(Ca)=6.36								
6166.439	2.521	–1.074	108.1	90.3	112.3		94.8	146.7
6455.598	2.523	–1.350	94.3	82.2	108.6	77.8	77.1	104.6
6499.650	2.523	–0.839	144.5	118.4	132.7		126.4	162.1
Sc II; log $\epsilon_{\odot}$(Sc)=3.10								
6320.851	1.500	–1.747	21.2	18.5	40.3			
Ti I; log $\epsilon_{\odot}$(Ti)=4.99								
5766.330	3.294	0.370	30.0	19.1	37.9	15.9	17.7	34.6
Cr I; log $\epsilon_{\odot}$(Cr)=5.67								
5787.965	3.323	–0.138	72.6	61.9	86.4	65.6	63.0	80.3
6925.202	3.450	–0.227	71.1				52.1	94.1
Fe I; log $\epsilon_{\odot}$(Fe)=7.67								
5543.937	4.218	–1.155	81.1	68.4	99.0		67.2	74.9
5638.262	4.221	–0.882	97.6	88.8	116.4	95.7	83.2	83.2
5806.717	4.608	–0.984	72.8	64.0	80.5	66.3	52.7	
5848.123	4.608	–1.282	71.2	62.8	80.9		47.0	39.5
5855.091	4.608	–1.681	39.9	32.4	47.7		21.4	21.2
5927.786	4.652	–1.243	58.2	50.2	65.1	50.1	40.8	39.6
5929.667	4.549	–1.332	57.3	51.1	66.8	48.8	40.3	40.4
5930.173	4.652	–0.347	123.2	90.3	138.0	99.7	91.1	90.0
5947.503	4.607	–2.059	23.2	32.4	41.2	13.7		
6078.491	4.796	–0.414	93.2	80.4	95.3	89.5	75.7	72.9
6078.999	4.652	–1.123	62.0	53.9	65.2	58.0	43.2	35.6
6094.364	4.652	–1.749	38.4	28.3	54.1	31.3	17.2	15.8
6098.280	4.559	–1.940	32.1	24.9	47.6	24.2	17.9	
6151.617	2.176	–3.486	79.3	76.7	97.6		60.8	69.6
6165.361	4.143	–1.645	65.3	60.6	70.9		57.3	41.2
6187.987	3.944	–1.740	70.4	62.2	80.4		50.9	48.8
6252.554	2.404	–1.867	182.0	155.9	191.8	151.5	199.2	188.1
6322.690	2.588	–2.503	128.1	105.6	152.6		88.1	111.2
6335.328	2.198	–2.432	146.4	128.5	161.2		143.4	147.6
6336.823	3.687	–0.896	170.3	143.0	173.5		141.7	143.4
6436.411	4.187	–2.538	25.6	19.9	35.6	18.6	15.0	
6469.213	4.835	–0.774	91.2	78.1	105.3	71.3	68.8	53.1
6699.162	4.593	–2.172	20.4	14.6	27.1			
6713.771	4.796	–1.606	38.0	39.3	45.6		24.2	
6725.353	4.104	–2.370	36.0	31.0	46.4		17.0	
6726.661	4.607	–1.200	63.5	57.7	71.8		46.1	39.2
6733.151	4.639	–1.594	48.2	43.4	49.5		31.0	
6820.369	4.639	–1.289	63.5	57.6	71.3	53.3	45.2	38.5

Table 6. Continued.

λ (Å)	χ (eV)	log gf (Morel 03)	EW (mÅ)[a] δ Eri	η Cep	γ Cep	HD 10780	HD 4628	61 Cyg
6843.648	4.549	–0.934	80.5	68.6	90.0	73.0	62.6	48.0
6857.243	4.076	–2.203	41.8	35.2	55.1	32.5	24.8	25.9
6861.937[b]	2.420	–3.990				34.6		
6862.492	4.559	–1.509	48.5	41.2	61.3	41.5	29.2	
7306.556	4.178	–1.684	63.8	62.2	85.9	52.8	48.9	40.3
7780.552	4.474	–0.175	181.0	146.7	173.2	150.0	202.0	137.5
7802.473	5.086	–1.493	31.0	22.2	35.9		24.7	
7807.952	4.992	–0.602	80.9	66.6	87.2	66.6	64.0	44.0
Fe II; log $\epsilon_{\odot}$(Fe)=7.67								
5991.376	3.153	–3.702	32.2	30.7	43.4		15.0	
6149.258	3.889	–2.858	30.6	32.0	37.5		15.2	
6247.562[b]	3.890	–2.770				39.8		
6432.680[b]	2.890	–3.758				33.8		
6456.383	3.904	–2.209	52.3	56.8	53.2	56.6	30.2	
Co I; log $\epsilon_{\odot}$(Co)=4.92								
6454.990	3.632	–0.233	38.2	34.8	58.5	24.2	17.2	
Ni I; log $\epsilon_{\odot}$(Ni)=6.25								
5805.213	4.168	–0.530	58.4	48.5	63.9	46.5	35.9	23.7
6111.066	4.088	–0.785	52.0	46.2	64.4	41.6	29.1	18.1
6176.807	4.088	–0.148	86.6	75.6	88.7		56.1	46.5
6186.709	4.106	–0.777	50.4	43.0	56.0			20.4
7555.598	3.848	0.069	145.2	118.1	135.1	113.4	108.3	80.2
Ba II; log $\epsilon_{\odot}$(Ba)=2.13								
5853.668	0.604	–0.758	83.2	82.3	88.8		53.3	56.1

[a] A blank indicates that the EW was not reliably measurable because of blends with telluric features or for an unsatisfactory Gaussian fit.
[b] The data for Fe I λ6861 and Fe II λ6432 are taken from Katz et al. (2003); data for Fe II λ6247 from Chen et al. (2003).